Catalysis Today 273 (2016) 259–265

Contents lists available at ScienceDirect

Catalysis Today

journal homepage: www.elsevier.com/locate/cattod

NiCe/γ-Al_2O_3 coated onto cordierite monoliths applied to Oxidative Dehydrogenation of Ethane (ODE)

P. Brussino, J.P Bortolozzi, V.G. Milt, E.D. Banús, M.A. Ulla *

Instituto de Investigaciones en Catálisis y Petroquímica, INCAPE (FIQ, UNL-CONICET), Santiago del Estero 2829, 3000 Santa Fe, Argentina

ARTICLE INFO

Article history:
Received 27 November 2015
Received in revised form 4 February 2016
Accepted 6 February 2016
Available online 29 March 2016

Keywords:
Nickel oxide
Nickel-cerium oxides
Cordierite monoliths
Oxidative dehydrogenation of ethane

ABSTRACT

The present work investigates the preparation of NiCe/γ-Al_2O_3 coated cordierite monoliths for oxidative dehydrogenation of ethane (ODE) reaction through a two steps procedure: the primer deposition of a γ-Al_2O_3 coating consisting in a mixture of micro and nanoparticles via the washcoating method and the latter incorporation of the active phase by impregnation. Moreover, a modification in these two steps was made: the suppression of some calcination steps to save energy in the manufacture process. The structured catalysts, named as Ni(X)Ce(Y)-M, where X = 13 or 19 wt%. Ni and Y = 5 or 8 wt%. Ce respectively, with respect to the alumina loading, were characterized by SEM/EDX, XRD, FTIR, LRS and XPS, and their catalytic activity was tested in the ODE reaction. Furthermore, their mechanical resistance to vibration was studied. Similar results corresponding to the un-promoted system are also presented for comparison. It was found that the co-impregnation of nickel and cerium was affected by the suppression of some calcinations: a preferential absorption of Ce rather than Ni occurred, generating at the end a catalytic coating with a higher Ce/Ni ratio than that of the precursor solution and a lower Ni loading than that of Ni(13)-M. On the other side, in the NiCe-based catalysts the properties of the active sites remained the same despite the increment in the active phase, at a fixed Ce/Ni nominal atomic ratio of 0.17. In the case of the Ni(19)Ce(8)-M system, although the Ni/Al atomic ratios were found lower than those of the nominal ones by EDX and XPS and ethylene selectivity decayed, ethane conversion resulted markedly higher, leading to an improved ethylene yield.

© 2016 Elsevier B.V. All rights reserved.

1. Introduction

Over recent years, research interests in ethylene production have increased due to its extensive utility. This compound is used as an intermediary to manufacture a wide variety of valuable products, polyethylene being the most significant one. Currently, ethene is produced via steam cracking of naphtha or ethane, an operation that consumes significant amounts of energy. The temperatures required for this process outweigh 800 °C and energy costs account for approximately 70% of production costs in typical ethane – or naphtha – based olefin plants [1].

Taking into account this scenario, the search for new alternatives to produce this compound becomes mandatory. The ODE reaction emerges as a promising route to achieve this goal because it presents several advantages with respect to the conventional process. In order to operate at relative low temperatures (400–500 °C) and to produce ethylene as the major product, an effective catalyst is required. This is reflected in the fact that the active sites of the catalytic formulation have to combine high activity and selectivity, i.e. to tailor the catalyst in such a way as to favor hydrogen abstraction and minimize oxygen insertion [2].

Several catalytic systems are being investigated for this reaction. An important group is based on transition metal oxides, in particular vanadium, molybdenum and nickel [3–10]. Bulk NiO has shown promising results as an ODE catalyst [9], but its selectivity needs to be improved. Recent studies have shown that this aspect can be enhanced either by supporting the active phase in a high surface area material [5,9] or adding a promoter to the catalytic formulation. In the former case, it has been demonstrated that dispersing NiO onto γ-Al_2O_3 improves the selectivity towards ethylene in this reaction [9]. In the latter case, the open literature reports a great variety of studies on promoters for NiO-based catalysts in powder form [11–15].

On the other hand, the efficiency of structured catalysts has proved to be higher than that of the corresponding powder forms, making their study of great interest if an industrial application is considered. In particular, monoliths are preferred due to their favorable properties with respect to selectivity, pressure drop and robustness [16].

* Corresponding author.
E-mail address: mulla@fiq.unl.edu.ar (M.A. Ulla).

http://dx.doi.org/10.1016/j.cattod.2016.02.055
0920-5861/© 2016 Elsevier B.V. All rights reserved.

The open literature offers little information about structured catalysts for oxidative dehydrogenation of ethane [17–22]. Ni-Ce-O catalysts have been reported as effective catalysts for the oxidative dehydrogenation of hydrocarbons (ODH) in powder and structured forms [17–19]. It has been demonstrated that the catalytic performance of nickel and cerium-based catalysts in the ODH reaction is dependent on the atomic Ce/Ni ratio [18,23–25]. Solsona et al. [15] studied Ni O-CeO_2 oxides as catalysts for ethane oxydehydrogenation. They varied the Ce/Ni atomic ratio from 0.02 to 5 and they achieved the best catalytic activities at 275 °C with the Ce/Ni atomic ratios of 0.083 and 0.17. On the other hand, Bortolozzi et al. [18] have studied NiCe/alumina-based deposited onto ceramic foams varying Ce/Ni atomic ratio from 0.05 to 0.25 and the Ce/Ni ratio of 0.17 demonstrated to be proper for the most efficient catalyst. Taking these results into account, in this work the selected Ce/Ni ratio was 0.17.

In a recent investigation [26] we studied two alumina supports for Ni/Al_2O_3 catalytic films onto cordierite monoliths via a two steps procedure: generating first the alumina layer by washcoating and incorporating latter the NiO phase through impregnation. One support consisted in nanoparticles of alumina and the other one was a mixture of nano and microparticles of alumina. Moreover, a modification in the washcoating and impregnation processes was made: some calcination stages were suppressed from the cycles in order to save energy in the preparation method. The system containing the mixture of nano and microparticles probed to be the most efficient one for the ODH reaction. With about Ni 15 wt% (with respect to γ-Al_2O_3) the catalysts exhibited more than 10% of conversion with ca. 80% selectivity to ethylene at 450 °C. Furthermore, the Ni loading of the systems was incremented to 25 wt% and it was found to improve ethane conversion with a minimal diminish in ethylene selectivity (not published). In the present work it is expected that these catalytic results, mainly the ethane conversion, could be further improved by the addition of cerium as a promoter.

Considering these previously obtained results, the aim of this work was to enhance the catalytic activity of the Ni/γ-Al_2O_3 monolithic catalyst by increasing the Ni loading and adding cerium as a promoter. To study its morphology and physicochemical aspects, SEM coupled with EDX, FTIR, DRX, LRS and XPS techniques were employed. Furthermore, in order to relate the physicochemical characteristics to the catalytic performance and offer further insights, a deep analysis of Raman and XPS results was performed.

2. Materials and methods

2.1. Preparation of the structured catalysts

Pieces of Cordierite monoliths (TENNECO®, 64 cells/cm^2) coated with NiCe/γ-Al_2O_3 with a theoretical nickel + cerium total loading of 15 and 25 wt% (with respect to alumina) were prepared by a two-step procedure. Firstly, an alumina layer was deposited onto the monoliths channels through the washcoating method. Cycles of immersion (1 min) – blowing (20 s) – drying (1 h) were carried out until the desired loading was reached, submerging the substrates into a suspension containing Al_2O_3 microparticles (Puralox® SBA-230, particle size of 45 μm), Al_2O_3 nanoparticles (colloidal suspension NYACOL® 20%wt), polyvinyl alcohol (PVA) and de-ionized water with the following molar composition 1: 0.09: 1.12: 3.15. Then, the Al_2O_3 coated monoliths were calcined in a muffle at 550 °C for 2 h. Later, the active phase was incorporated by immersion in a 0.43 M solution of $Ni(NO_3)_2$ and $Ce(NO_3)_3$, with a nominal Ce/Ni atomic ratio of 0.17. Finally, the samples were calcined at 550 °C for 2 h. These structured catalysts were designated as Ni(X)Ce(Y)-M, where X = wt% of Ni and Y = wt% of Ce with respect to alumina and M represents the cordierite monoliths.

2.2. Characterization of the structured catalysts

The morphology in the inner channel walls and in the cross sections was observed by Scanning Electron Microscopy (SEM) with a ZEISS instrument SUPRA 40 model, which was operated with an acceleration voltage of 20 kV. The apparatus was equipped with an EDS detector, Oxford Instruments, for EDX semiquantitative analysis. A FEG (Field Emitter Gun) electron source was also employed to study the elemental chemical composition and the elements distribution (mapping). Samples were glued to the sample holder with Ag painting and then coated with a thin layer of Pt, in order to improve the quality of the images.

The anchorage of the catalytic films to the monolithic substrates was tested by submitting the monoliths to an ultrasonic bath (Testlab TB04 equipment, 40 kHz and 160 W) for 90 min in acetone and measuring the weight loss. The adherence percentage was referred to the added catalytic layer.

X-ray diffraction (XRD) was used to elucidate the crystalline phases present in the catalytic formulations. The diffractograms were obtained with a Shimadzu XD-D1 instrument with monochromator using Cu Kα radiation at a scan rate of 2°/min, from 2θ = 20 to 80°. The monolith pieces were cut along the channels and they were held in a special holder for the analysis.

Fourier Transform Infrared Spectroscopy (FTIR) was performed in order to identifythe functional groups. The IR wafers were prepared by mixing KBr powder with the particles obtained by scrapping the inner channels of the monolith pieces (ca. 1% sample in KBr). A Shimadzu IR Prestige-21 spectrometer was used to obtain the infrared spectra. All spectra were acquired at 8 cm^{-1} of resolution and accumulation of 40 scans.

In addition, Laser Raman Spectroscopy (LRS) was performed to identify the components present in the samples and study their frequency modes. The spectra were recorded using a LabRam spectrometer (Horiba-Jobin-Yvon) coupled to an Olympus confocal microscope (a 50x objective lens was used for simultaneous illumination and collection), equipped with a CCD detector cooled to about −70 °C using the Peltier effect. The excitation wavelength was in all cases 532.13 nm (Spectra Physics diode pump solid state laser). The laser power was set at 30 mW.

The elemental composition at surface level and the chemical state of the systems were investigated by X-ray Photoelectron Spectroscopy (XPS). The measurements were performed in a SPECS equipment with a hemispherical PHOIBOS 150 analyzer operated in the FAT mode. The spectra were obtained with pass energy of 30 eV and Mg-Kα X-ray source power of 200W. The samples were evacuated in vacuum at 10^{-3} mbar and 200 °C for 10 min in the chamber. Later, they were evacuated for 2 h in ultra high vacuum. The peak fitting was performed with the CASAXPS software using C 1s at 284.6 eV as a reference.

2.3. Catalytic activity measurements

The oxidative dehydrogenation of ethane (ODE) was performed in a flow system operated between 300 and 450 °C. The feed composition was 6% O_2 and 6% C_2H_6 diluted in He. The weight of the tested catalysts was ~0.4 g (metal oxides + alumina). The W/F ratio was fixed at 0.48 g s/cm^3. A second part of the experiments was conducted at constant temperature (450 °C) with variable W/F ratio. Reactants and products were quantified with a gas chromatograph (Shimadzu® GC 2014) equipped with a packed column (HayeSep D®). Closure of the carbon mass balance was 100 ± 2%. Carbon monoxide was not detected in the products stream after the reaction. The ethane conversion (X_{ethane}) and the selectivity towards ethylene ($S_{ethylene}$) were based on the carbon mass balance [18].

3. Results and discussion

3.1. Preparation of the structured catalysts

To deposit approximately 300 mg of the alumina coating, five or six cycles were required. The weight gain was approximately constant after the complete sequence and standard deviations did not overcome 30 mg in all cases.

The addition of the active phases in each case is shown in Table 1. The three prepared systems required intermediate calcinations in order to reach the desired Ni or NiCe loading because, every 2 or 3 cycles, the incorporated precursor dissolved back into the solution when the immersion was carried out. After calcination, the nickel and cerium nitrates decomposed into the corresponding oxides. The Ni/Al nominal atomic ratios were calculated for each sample considering that Al comes from Al_2O_3 only and not from cordierite and they were around 0.11–0.16 (Table 1). Although the Ce/Ni nominal atomic ratios were set to 0.17, the values found with EDX were higher: 0.25–0.28 (Table 2).

3.2. Morphology, elements distribution and chemical analysis of the monolithic catalysts

Cordierite monolith walls have several macropores, with sizes around 10 μm, distributed along the structure (Figs. 1a and 2a). In both systems, Ni(13)Ce(5)-M and Ni(19)Ce(8)-M, the totality of these macropores are covered by the alumina particles (Figs. 1a and 2a). This is related to what is observed through the mapping images where Si (constitutive element of cordierite) is visible inside the walls rather than in the channels (Figs. 1b and 2b). Besides, the active phase is homogeneously distributed along the channels and only small amounts of nickel and cerium are visualized inside the walls in both systems (1c,d and 2c,d).

Furthermore, the promoted systems exhibited a wrinkled morphology of the catalytic films compared to that of the Ni(13)-M catalyst (not shown). This feature became more noticeable when the NiCe loading increased.

Table 2 displays the average atomic ratios obtained by EDX for two areas of each sample: the centre and the edge of the channel. In all systems, practically neither Mg nor Si (constitutive elements of cordierite) was detected, either along the channel or in the edge zones. This observation indicates that the catalytic films were thicker than 3 μm (analysis depth) and confirms what was observed by mapping and SEM micrographs. The Ni/Al atomic ratios resulted similar to the nominal ones and the standard deviations did not overcome the value of 0.02. These results confirm that nickel was homogeneously distributed along the channel in all samples, in agreement with the mapping images. The Ce/Ni ratios were similar in both samples and they were higher than the theoretical ones, indicating a preferential absorption of Ce rather than Ni on the alumina surface. This could be related to either the solubility of the metal precursors in water and/or metallic ion preferential adsorption. In the former situation, nickel nitrate hexahydrate is more soluble in water than cerium nitrate hexahydrate. On the other hand, preferential adsorption of Ce on the alumina surface could also take place.

3.3. Mechanical stability

After 90 min in an ultrasonic bath, the structured systems presented adherences over 95% (Table 1). The anchorage of the support (alumina) to the cordierite was also studied, being around 96%. The percentages increased with the amount of active phase incorporated. This is probably related to the number of calcinations experienced by each system. After more calcination stages, a better anchorage was obtained.

3.4. Physico-chemical characterization

The Raman spectra of the catalysts (Fig. 3) show an asymmetrical broad band at 500–600 cm^{-1} corresponding to stretching modes of Ni-O bonds (first-order phonons). This signal, located at 570 cm^{-1} for the Ni(13)-M system, shifted to higher frequencies with respect to that of bulk NiO (centered at ~500 cm^{-1}), thus indicating a strong interaction between nickel species and the support. A shoulder at ~490 cm^{-1} verifies the non-stoichiometry property of the NiO film [27]. For the promoted systems, the main band is broader. This is probably related to the presence of two types of nickel interactions, one with alumina and the other with ceria.

The spectra of the systems containing Ce present three additional signals. The peak at 462 cm^{-1} corresponds to the fluorite-type structure of CeO_2 [28] and it is due to the Raman active F_{2g} mode [29,30]. This vibration mode is related to the oxygen atoms surrounding the Ce^{4+} cation [18]. In pure CeO_2, this signal is observed at 465 cm^{-1}; then, the slight red shift observed indicates a little decrease in the Ce-O bond strength due to the doping of ceria with Ni^{2+} cations. In order to maintain the charge neutrality, when Ni^{2+} incorporates into the ceria network replacing some Ce^{4+} cations, an oxygen vacancy must be generated. According to C. Tang et al. [31], with the doping of Ni^{2+} the following process probably takes place:

$$O^{2-} - Ce^{4+} - O^{2-} - Ce^{4+} \overset{Ni^{2+}\ doping}{\rightarrow} O^{2-} - Ce^{4+} - \blacksquare - Ni^{2+} + 2e^- + O$$

Not only the oxygen vacancy (represented by■) is formed, but also two electrons. These electrons can combine with the oxygen vacancies to form− anionic vacancies which function as molecular oxygen reservoir, giving these catalysts the property of oxygen storage due to the presence of CeO_2.

The formation of a solid solution is confirmed by the appearance of a well-defined band at 227 cm^{-1} since it is closely related to lattice defects originated from the oxygen vacancies. Moreover, the band at 637 cm^{-1} is attributed to modifications of the oxygen sublattice due to the introduction of nickel into the ceria network, further confirming the modification of the M-O bonding symmetry and the formation of the Ni-Ce-O solid solution. These oxygen vacancies are related to the improvement of the redox properties of Ce^{+4}/Ce^{+3} [32,33].

The diffractograms of the structured catalysts (not shown) revealed the presence of γ-Al_2O_3 in all samples by the evident distortion of the cordierite peaks where the alumina signals should appear. The diffractions of the CeO_2 crystallites as well as the ones of NiO were not detected, indicating that the crystallite sizes of both systems should be in the order of a few nanometers. Besides, it means that there is an elevated dispersion of these crystallites onto the alumina surface.

FTIR spectra (not shown) of the catalysts did not show a band at 1385 cm^{-1} indicating that the nitrates decomposed completely into oxides. A broad band appeared at 3460 cm^{-1} and another one at 1634 cm^{-1}, both corresponding to the vibration modes of water physically adsorbed in the support. The M-O vibrational modes were spotted in the 400–800 cm^{-1} region, where M refers to Ni, Ce and the metals present in the cordierite (Al, Mg and Si).

The surface properties of the structured catalysts were analyzed by XPS. The Ni $2p_{3/2}$ spectrum is shown in Fig. 4a. The fact that the main line does not show a double peak and that this signal is not asymmetrical lets us infer that the NiO (Ni^{2+}) coverage is a few nanometers thick and that the Ni^{2+} species are highly dispersed in the alumina coating [34]. The main signal for the NiCe catalysts and Ni catalyst are positioned at 855.7 and 856.2 eV respectively. Gen-

Table 1
Main features of the prepared structured catalysts.

Sample	Cycles (Ni/NiCe solution)	Intermediate calcination	$Ni/Al)_T$	$Ce/Ni)_T$	Adherence (%)[a]
Ni(13)-M	9	2	0.11	–	97.40
Ni(13)Ce(5)-M	5	2	0.11	0.17	96.95
Ni(19)Ce(8)-M	9	4	0.16	0.17	99.48

T = theoretical.
[a] Referred to the added catalyst loading.

Table 2
Elemental distributions on different monolith zones for the three structured catalysts.

	Mg/Al	Si/Al	Ni/Al	Ce/Ni
	Ni(13)-M; $(Ni/Al)_T = 0.11$			
Channel centre	ND	ND	0.08 ± 0.01	–
Channel edge	ND	ND	0.12 ± 0.02	–
	Ni(13)Ce(5)-M; $(Ni/Al)_T = 0.11$, $(Ce/Ni)_T = 0.17$			
Channel centre	ND	ND	0.07 ± 0.02	0.28 ± 0.03
Channel edge	ND	ND	0.03 ± 0.02	0.28 ± 0.02
	Ni(19)Ce(8)-M; $(Ni/Al)_T = 0.16$, $(Ce/Ni)_T = 0.17$			
Channel centre	0.00 ± 0.01	0.01 ± 0.01	0.10 ± 0.02	0.25 ± 0.05
Channel edge	0.01 ± 0.01	0.02 ± 0.02	0.08 ± 0.01	0.25 ± 0.05

ND: not detected; T: theoretical.

erally, the binding energy reported for bulk NiO is about 854.0 eV, consequently there is a strong interaction between Ni^{2+} and Ce^{4+} species and the support, in agreement with the Raman results. The addition of the promoter modifies the environment of nickel at the alumina surface because the BEs corresponding to the Ce-containing catalysts resulted slightly shifted to lower frequencies. This indicates that the nickel-alumina interaction is probably weakened by the introduction of cerium [8,35].

The spectra for O 1s are shown in Fig. 4b. The main peak is positioned at 529.7 eV for the Ce-promoted systems and at 530.3 eV for the un-promoted system. This signal is attributed to the lattice oxygen (O_L) of the metal oxides. In addition, a peak at higher binding energy (O_V), 531.3–531.9 eV, is present in all catalysts. The origin of this signal is not clear yet, but it could represent defective oxygen, i.e. oxygen atoms in the vicinity of Ni and Ce vacancies, absorbed oxygen, oxygen in carbonates or hydroxyl groups [30,36]. The ratios of the areas O_V/O_L were calculated for the three systems and they proceed along the following order: Ni(19)Ce(8)-M = Ni(13)Ce(5)-M > Ni(13)-M. The catalysts containing Ce would have the same amount of oxygen vacancies because they have a similar Ce/Ni ratio (EDX). These systems also have a higher ratio than the un-promoted one. This is consistent with the Raman results (Fig. 3, bands at 227 and 631 cm^{-1}), in which it can be that nickel cations replace some Ce^{4+} cations generating oxygen vacancies. These electrophilic oxy-

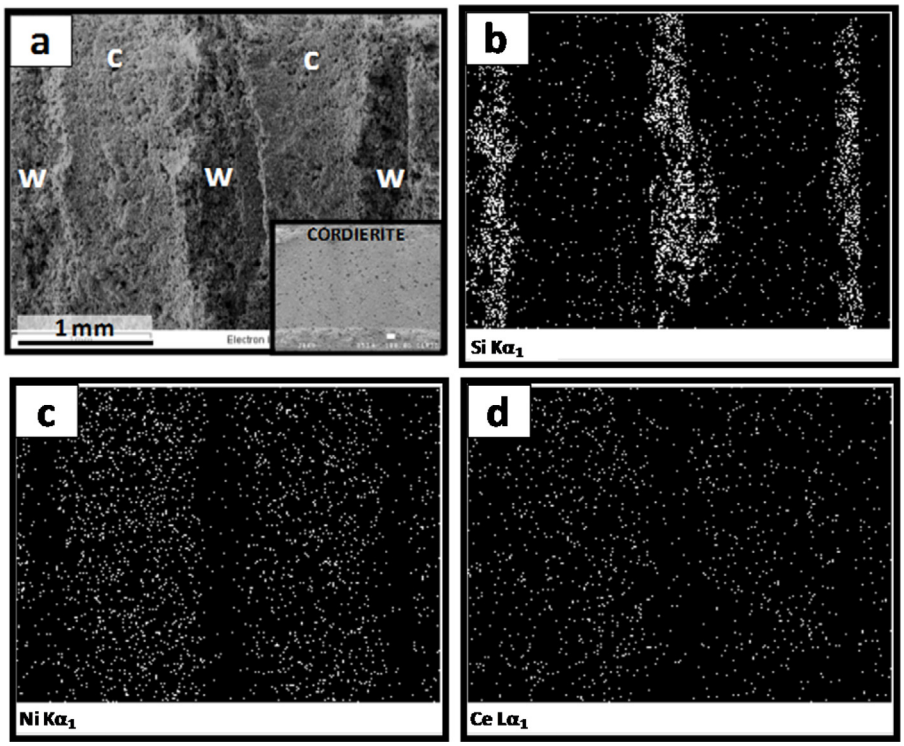

Fig. 1. SEM micrograph and mapping images of the Ni(13)Ce(5)-M system. (a) SEM micrograph, c: channel, w: wall; cordierite micrograph for comparison. Mappings: (b) Si $K\alpha_1$, (c) Ni $K\alpha_1$ and (d) Ce $L\alpha_1$.

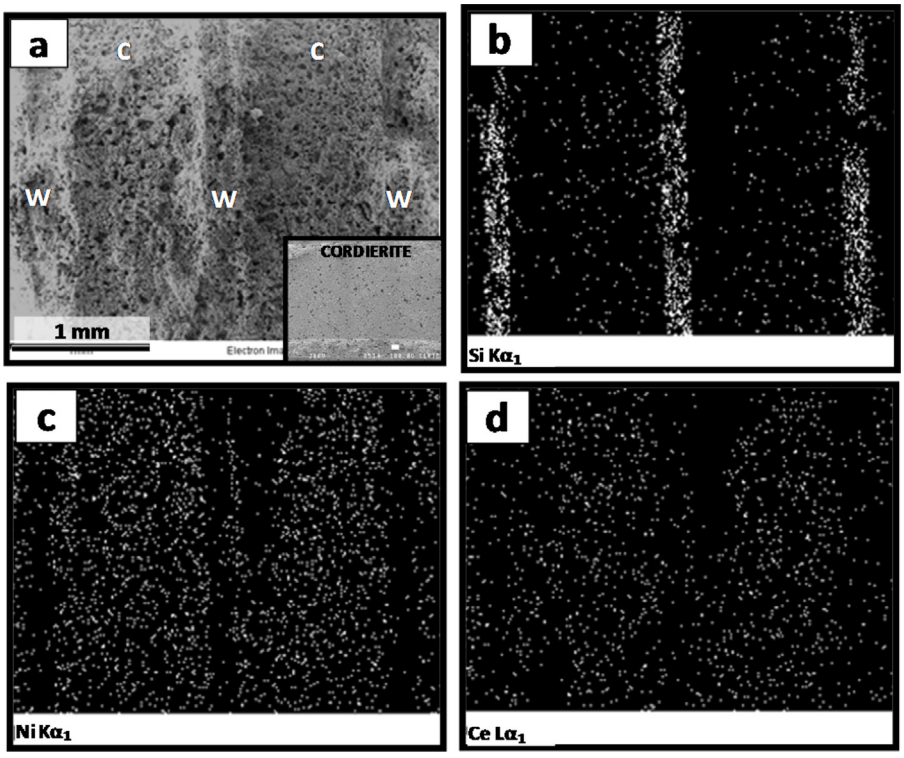

Fig. 2. SEM micrograph and mapping images of the Ni(19)Ce(8)-M system. (a) SEM micrograph, c: channel, w: wall; cordierite micrograph for comparison. Mappings: (b) Si $K\alpha_1$, (c) Ni $K\alpha_1$ and (d) Ce $L\alpha_1$.

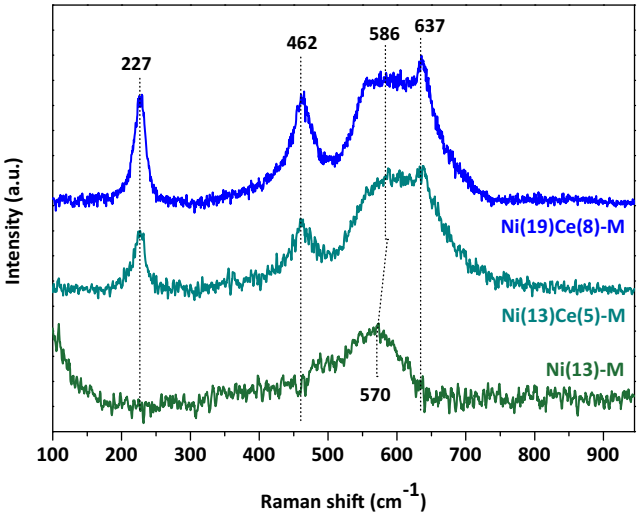

Fig. 3. Raman spectra of the structured catalysts.

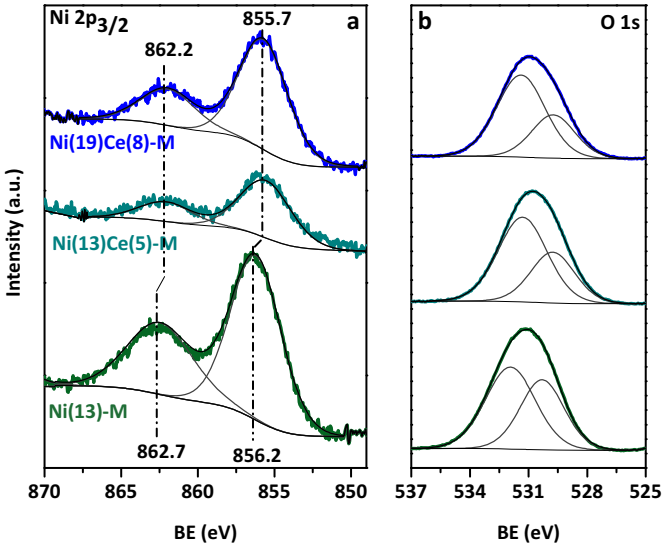

Fig. 4. XPS spectra of the structured catalysts in the Ni $2p_{3/2}$ and O 1s regions.

gen species have proved to turn the NiO-based catalysts in the ODE reaction very unselective to ethylene [11]. Taking this phenomenon into account, the increase in defective oxygen in the promoted catalysts could result in a decrease of ethylene selectivity.

The Ni $2p_{1/2}$ signals are overlapped with the Ce $3d_{5/2}$ ones (Fig. 5). The Ni $2p_{1/2}$ peak is at 873.7 eV for Ni(13)Ce(5)-M and 873.4 eV for Ni(19)Ce(8)-M, each one with its satellite at ~6 eV higher BE. The ΔBE between the main signals of Ni $2p_{3/2}$ and Ni $2p_{1/2}$ is around 17.8 eV, confirming the strong interaction between the nickel species and alumina in the promoted catalysts. In the case of the cerium-free sample, the Ni $2p_{1/2}$ main signal appears at 873.8 eV (not shown) and the difference between this one and Ni $2p_{3/2}$ is 18 eV. This also indicates that a significant amount of free NiO (Ni^{2+}) was not present on the surface, since the value reported for bulk NiO is 18.6 eV [8].

It is worth mentioning that the amount of cerium in the catalysts is low, consequently the Ce 3d spectra are noisy and the curve fitting difficult (Fig. 5). The best fit, taking into account the minimal error, was found only with the presence of Ce^{4+}. It is possible that some amount of Ce^{3+} is present but if it were, it would be minimal. Peaks named as *u* arise from $3d_{3/2}$ photoemissions whereas the ones labeled as *v* are associated with $3d_{5/2}$ photoemissions. The BEs associated with the signals are in agreement with the corresponding values published in the literature [37–39].

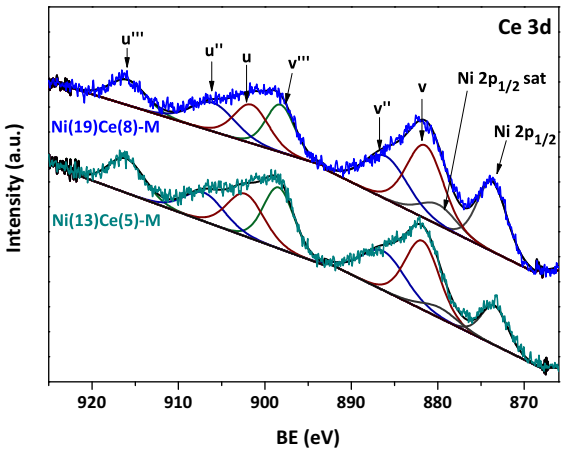

Fig. 5. XPS spectra of the structured catalysts in the Ce 3d region.

The surface Ce/Ni atomic ratios obtained for the promoted systems, Ni(13)Ce(5)-M and Ni(19)Ce(8)-M, were 1 and 0.48 respectively whereas the bulk Ce/Ni ratios obtained by EDX were 0.28 and 0.25 (Table 2). A surface enrichment of cerium in the catalysts (up to 5 nm) is evidenced by these values. These results are in good agreement with thermodynamic considerations, which demonstrate that the surface for most multi-component systems becomes enriched in the constituent that has the lowest surface energy. Therefore, the surface free energies of CeO_2 and NiO are 0.7 and 3.05 J/m^2, respectively [40]. Besides, the surface Ce/Ni value for the sample with 9 impregnation cycles, Ni(19)Ce(8)-M, was 0.48 and it was lower than that of Ni(15)Ce(5)-M with 5 cycles, which was 1. This difference on both promoted systems would be attributed to the impregnation procedure of the active phases. The same precursor solution was used for all the immersion steps and after each step an enrichment of Ni in the solution could be expected due to the preferential Ce adsorption. As a result, increasing the number of impregnation steps would decrease the Ce/Ni atomic ratio. These results are in line with what was analyzed by EDX (Table 2).

In the promoted catalysts, the Ni/Al ratio also showed a decrease of surface nickel, whereas for the un-promoted one this ratio was the same as the one found by EDX. The decrease of nickel amount on the surface and therefore the enrichment of cerium could negatively affect the catalyst selectivity.

The active species properties and their distribution on the catalytic coatings play a significant role in the catalytic performance. Briefly, the main features in the structured catalysts prepared in this work are the following:

The NiO particles are well dispersed onto the Al_2O_3 layer, having a strong interaction with the support surface. In the case of the Ce-promoted NiO monoliths, part of Ni interacts with the Ce-O structure, modifying its chemical environment and increasing the number of oxygen vacancies.

– Although the bulk Ni/Al ratios determined by EDX are slightly lower for Ni(19)Ce(8)-M and Ni(13)Ce(5)-M compared with the theoretical ratios, this ratio for Ni(13)-M is quite similar (Table 2). In contrast, the bulk Ce/Ni ratios on the Ce promoted NiO monoliths are always higher than the theoretical one. Moreover, this enrichment is higher on the surface outlayer.

3.5. Catalytic behavior in the ODH ethane reaction

Fig. 6a shows the ethane conversion as a function of reaction temperature. The addition of the promoter remarkably increased the ethane conversion, reaching ~35% at 450 °C the Ni(19)Ce(8)-M system. Therefore, the Ni species that are interacting with Ce contribute as highly active sites.

The selectivity towards ethylene at constant temperature (450 °C) is displayed in Fig. 6b, where the reaction scheme is also shown. The trend lines obtained for the catalysts can be explained by this reaction scheme. The intercept of these lines with *y* axis reflects the behavior of the catalysts in the direct oxidation of ethane to carbon dioxide, whereas the slope indicates its tendency to produce CO_2 from the just formed ethylene. The selectivity towards ethylene was diminished by the incorporation of Ce to the catalytic formulation, indicating that the direct oxidation of ethane is a little more favored in these cases. This is explained through the oxidizing power of CeO_2 [15,18]. On the other hand, the slopes of the lines remained the same compared to the system without promoter, indicating that the tendency of the produced ethylene to form carbon dioxide has not been modified. Since these slopes were not highly marked, the oxidation of ethylene is slightly favored in all cases.

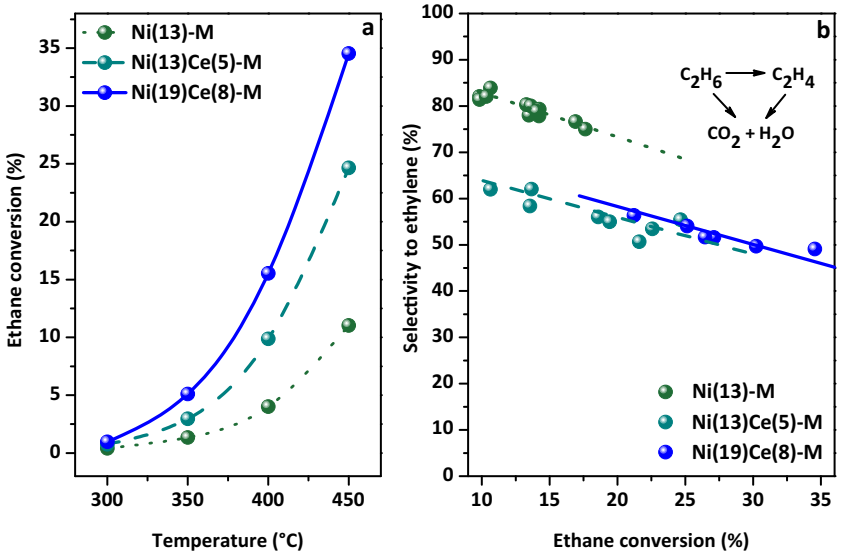

Fig. 6. Catalytic performance of the structured catalysts: (a) ethane conversion as a function of reaction temperature, W/F = 0.48 g s/cm^3 and (b) selectivity to ethylene at 450 °C and variable W/F.

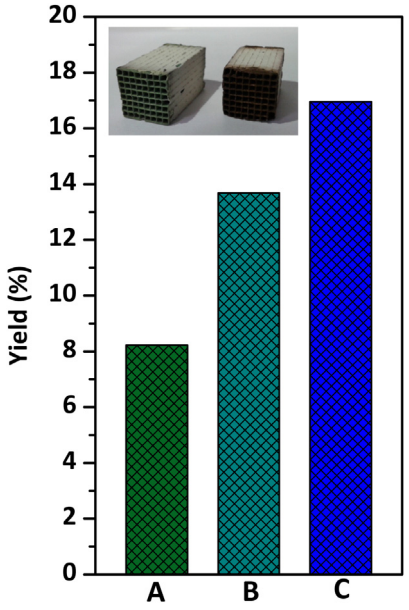

Fig. 7. Yield of ethylene at 450 °C corresponding to each structured catalyst: (A) Ni(13)-M, (B) Ni(13)Ce(5)-M and (C) Ni(19)Ce(8)-M.

The Ni(19)Ce(8)-M catalyst exhibited higher conversion than Ni(13)Ce(5)-M, because the former structured catalyst had a higher Ni/Al ratio. Moreover, the characteristic active sites of both promoted systems are somehow the same and it is confirmed by their similar values of selectivity towards ethylene. The ethylene yield at 450 °C corresponding to each catalyst is displayed in Fig. 7. It can be seen that the incorporation of the promoter to the monometallic catalyst leads to a practically doubled yield of ethylene, although the selectivities resulted lower (Fig. 6b).

The catalytic performances of NiCe coated onto Al_2O_3 foams were reported by Bortolozzi et al. [18]. The catalytic layers were obtained with different Ce/Ni ratios and tested on ODE reaction, using the same operating conditions as this work. The estimated yield for the Ni-Ce foam with two EDX Ce/Ni ratios, 0.18 and 0.25, were 18.62 and 14.62, respectively. Both values are comparable with those obtained for the promoted system on this work (Fig. 7). However, the Ni/Al ratio for the foam samples was almost twice as high as that of monolith samples. Our next task is to increase the number of active sites maintaining the catalytic properties.

4. Conclusions

The obtained catalytic coatings exhibit excellent mechanical adherence and interesting catalytic performance even though some calcinations were removed from the two-step procedure. Moreover, the active phases are homogeneously distributed along the monoliths channels strongly interacting with the support. This indicates that the method employed for the deposition of the catalyst is adequate.

The consecutive impregnation of Ce and Ni onto the Al_2O_3 layer with less calcination steps privileges Ce adsorption, generating at the end a catalytic coating with a higher Ce/Ni ratio than that of the precursor solution and a lower Ni loading than that of Ni(13)-M. Moreover, a marked increment of the Ce/Ni ratio values in the outlayer of the coating was observed by XPS technique; probably due to the fact that CeO_2 has a lower surface energy than NiO.

When ceria is present in the catalysts, two species of nickel are formed: one of them interacting with alumina (as the ones in the un-promoted system) and another one interacting with cerium species. The latter constitutes a different active site that contributes to enhance the catalytic performance. The properties of these active sites remains the same despite the increment of the number of impregnation cycles needed to achieve the Ni-Ce loading of the Ni(19)Ce(8)-M system.

Acknowledgments

The authors acknowledge the financial support received from ANPCyT, CONICET and UNL. Thanks are also given to ANPCyT for the purchase of the SPECS multitechnique analysis instrument (PME8-2003) and the Grant PME 87-PAE 36985 to purchase the RAMAN Instrument.

References

[1] T. Ren, M. Patel, K. Blok, Energy 31 (2006) 425–431.
[2] C.A. Gärtner, A.C. van Veen, J.A. Lercher, ChemCatChem 5 (2013) 1–23.
[3] D. Shee, G. Deo, Catal. Lett. 124 (2008) 340–351.
[4] M.D. Argyle, K. Chen, A.T. Bell, E. Iglesia, J. Catal. 208 (2002) 139–149.
[5] G. Tsilomelekis, A. Christodoulakis, S. Boghosian, Catal. Today 127 (2007) 139–147.
[6] E. Heracleous, M. Machli, A.A. Lemonidou, I.A. Vasalos, J. Mol. Catal. A 232 (2005) 29–39.
[7] N. Haddad, E. Bordes-Richard, L. Hilaire, A. Barama, Catal. Today 126 (2007) 256–263.
[8] E. Heracleous, A.F. Leeb, K. Wilson, A.A. Lemonidou, J. Catal. 231 (2005) 159–171.
[9] Z. Skoufa, G. Xantri, E. Heracleous, A.A. Lemonidou, Appl. Catal. A 471 (2014) 107–117.
[10] H. Zhu, H. Dong, P. Laveille, Y. Saih, V. Caps, J. Basset, Catal. Today 228 (2014) 58–64.
[11] B. Savova, S. Loridant, D. Filkova, J.M.M. Millet, Appl. Catal. A 390 (2010) 148–157.
[12] B. Solsona, J.M. López Nieto, P. Concepción, A. Dejoz, F. Ivars, M.I. Vázquez, J. Catal. 280 (2011) 28–39.
[13] E. Heracleous, A.A. Lemonidou, J. Catal. 270 (2010) 67–75.
[14] B. Solsona, P. Concepción, B. Demicol, S. Hernández, J.J. Delgado, J.J. Calvino, J.M. López Nieto, J. Catal. 295 (2012) 104–114.
[15] B. Solsona, P. Concepción, S. Hernández, B. Demicol, J.M. López Nieto, Catal. Today 180 (2012) 51–58.
[16] J.A. Moulijn, A. Stankewicz, F. Kapteijn, Chem. Sustainable Dev. 11 (2003) 3–9.
[17] B. Chu, L. Truter, T.A. Nijhuis, Y. Cheng, Catal. Sci. Technol. 5 (2015) 2807–2813.
[18] J.P. Bortolozzi, L.B. Gutierrez, M.A. Ulla, Catal. Commun. 43 (2014) 197–201.
[19] J.P. Bortolozzi, T. Weiss, L.B. Gutierrez, M.A. Ulla, Chem. Eng. J. 246 (2014) 343–352.
[20] J.P. Bortolozzi, E.D. Banuís, V.G. Milt, E.E. Miro, Ind. Eng. Chem. Res. 53 (2014) 17570–17579.
[21] J.P. Bortolozzi, L.B. Gutierrez, M.A. Ulla, Appl. Catal. A 452 (2013) 179–188.
[22] J.A. Santander, E. Loípez, G.M. Tonetto, M.N. Pedernera, Ind. Eng. Chem. Res. 53 (2014) 11312–11319.
[23] L. Jalowiecki-Duhamel, A. Ponchel, C. Lamonier, A. D'Huysser, Y. Barbaux, Langmuir 17 (2001) 1511–1517.
[24] P. Boizumault-Moriceau, A. Pennequin, B. Grzybowska, Y. Barbaux, Appl. Catal. A 245 (2003) 55–67.
[25] Y. Liu, L. Wang, M. Chen, J. Xu, Y. Cao, H. He, K. Fan, Catal. Lett. 130 (2009) 350–354.
[26] P. Brussino, J.P. Bortolozzi, V.G. Milt, E.D. Banús, M.A. Ulla, Ind. Eng. Chem. Res. 55 (2016) 1503–1512.
[27] S. Lee, H.M. Cheong, N. Park, C.E. Tracy, A. Mascarenhas, D.K. Benson, S.K. Deb, Solid State Ionics 140 (2001) 135–139.
[28] I. Kosacki, T. Suzuki, H.U. Anderson, P. Colomban, Solid State Ionics 149 (2002) 99–105.
[29] G.W. Graham, W.H. Weber, C.R. Peters, R. Usmen, J. Catal. 130 (1991) 310–313.
[30] S. Kanakaraju, S. Mohan, A.K. Sood, Thin Solid Films 305 (1997) 191–195.
[31] C. Tang, J. Lia, X. Yaoc, J. Sun, Y. Cao, L. Zhang, F. Gao, Yu Deng, Lin Dong, Appl. Catal. A 494 (2015) 77–86.
[32] F. Liang, Y. Yu, W. Zhou, X. Xua, Z. Zhu, J. Matter. Chem. A 3 (2015) 634–640.
[33] X. Liu, Y. Zuo, L. Li, X. Huang, G. Li, RSC Adv. 4 (2014) 6397–6406.
[34] S. Palacín, A. Gutiérrez, I. Preda, M. Hernández-Vélez, R. Sanz, J.A. Jiménez, L. Soriano, Appl. Surf. Sci. 254 (2007) 278–280.
[35] F. Meng, Z. Li, J. Liu, X. Cui, H. Zheng, J. Nat. Gas Sci. Eng. 23 (2015) 250–258.
[36] D.T. Nguyen, A. Ferrec, J. Keraudy, M. Richard-Plouet, A. Goullet, L. Cattin, L. Brohan, P.-Y. Jouan, Surf. Coat. Technol. 250 (2014) 21–25.
[37] C. Anandan, P. Bera, Appl. Surf. Sci. 283 (2013) 297–303.
[38] C.A. Chagas, E.F. de Souza, R.L. Manfro, S.M. Landi, M.M.V.M. Souza, M. Schmala, Appl. Catal. B 182 (2016) 257–265.
[39] E. Bêche, P. Charvin, D. Perarnau, S. Abanades, G. Flamant, Surf. Interfase Anal. 40 (2008) 264–267.
[40] H.M. AbdelDayem, M. Faiz, H.S. Abdel-Samad, S.A. Hassan, J. Rare Earths 33 (2015) 611–618.